

Article

Evaluation of the Thermal Behavior, Synergistic Catalysis, and Pollutant Emissions during the Co-Combustion of Sewage Sludge and Coal Gasification Fine Slag Residual Carbon

Yang Guo ^{1,2}, Jianjun Wu ^{1,2}, Wenke Jia ^{1,2}, Fanhui Guo ^{1,2}, Guofeng Qiu ^{1,2}, Rumeng Wang ^{1,2}, Yixin Zhang ^{2,3,*} and Baiqian Dai ^{4,5,*}

- ¹ School of Chemical Engineering and Technology, China University of Mining and Technology, Xuzhou 221116, China; cumt-guoyang@cumt.edu.cn (Y.G.); jjuw@163.com (J.W.); jwk0812@163.com (W.J.); cumtgfh@163.com (F.G.); ts20040045a31@cumt.edu.cn (G.Q.); rumengwang@cumt.edu.cn (R.W.)
- ² National Engineering Research Center of Coal Preparation and Purification, China University of Mining and Technology, Xuzhou 221116, China
- ³ Shandong Xuanyuan Scientific Engineering and Industrial Technology Research Institute Co., Ltd., Longgu, Juye, Heze 274918, China
- ⁴ Department of Chemical Engineering, Monash University, Clayton, VIC 3800, Australia
- ⁵ Monash Suzhou Research Institute, SIP, Suzhou 215028, China
- * Correspondence: yixinzhang@cumt.edu.cn (Y.Z.); Bai-Qian.Dai@monash.edu (B.D.)



Citation: Guo, Y.; Wu, J.; Jia, W.; Guo, F.; Qiu, G.; Wang, R.; Zhang, Y.; Dai, B. Evaluation of the Thermal Behavior, Synergistic Catalysis, and Pollutant Emissions during the Co-Combustion of Sewage Sludge and Coal Gasification Fine Slag Residual Carbon. *Catalysts* **2021**, *11*, 1142. <https://doi.org/10.3390/catal11101142>

Academic Editor: Giuseppe Pantaleo

Received: 22 August 2021

Accepted: 21 September 2021

Published: 23 September 2021

Publisher's Note: MDPI stays neutral with regard to jurisdictional claims in published maps and institutional affiliations.



Copyright: © 2021 by the authors. Licensee MDPI, Basel, Switzerland. This article is an open access article distributed under the terms and conditions of the Creative Commons Attribution (CC BY) license (<https://creativecommons.org/licenses/by/4.0/>).

Abstract: The conversion of solid waste into energy through combustion is sustainable and economical. This study aims to comprehensively evaluate and quantify the co-combustion characteristics, synergistic catalysis, and gaseous pollutant emission patterns of sewage sludge (SS) and coal gasification fine slag residual carbon (RC) as well as their blends through thermogravimetry coupled with mass spectrometry (TG-MS). The results showed that the co-combustion of SS and RC can not only improve the ignition and burnout property but also maintain the combustion stability and comprehensive combustion performance at a better level. The kinetic analysis results showed that a first-order chemical reaction and three-dimensional diffusion are the reaction mechanisms during the co-combustion of SS and RC. The synergistic catalysis between SS and RC can well explain the changes in activation energy and reaction mechanism. Furthermore, the blending ratio of SS is recommended to be maintained at 40% because of the lowest activation energy ($E_a = 81.6$ kJ/mol) and the strongest synergistic effect ($X_i = 0.36$). The emission of gaseous pollutants is corresponding to the primary combustion stages of SS, RC, and their blends. In co-combustion, the NH_3 , HCN, NO_x , and SO_2 emissions gradually rise with the increase of SS proportion in the blends due to the high content of organic compounds in SS.

Keywords: sewage sludge; coal gasification fine slag; co-combustion; kinetics; synergistic catalysis

1. Introduction

Sewage sludge is the by-product of urban sewage treatment plants [1]. In China, about 30 million tons of sewage sludge (80% moisture content) is produced every year, and this is still growing [2]. Sewage sludge is considered to be a kind of solid waste, which contains numerous pollutants, such as bacteria, viruses, dioxins, and heavy metals. [3,4]. Therefore, a simple landfill or dumping of sewage sludge will occupy precious land resources and bring potential harm to the ecological environment [5,6]. However, sludge incineration can not only destroy bacteria, viruses, and toxic organic matter to minimize environmental pollution but also recover the energy in sewage sludge [7].

Sewage sludge has the characteristics of high volatile content, high ash content, and low calorific value, which has an adverse effect on the combustion of sewage sludge, and therefore the combustion efficiency and stability of sewage sludge are poor. The co-combustion of sludge and other solid fuels is a feasible solution that can effectively

improve the combustion performance [8]. To date, there have been many research reports regarding the co-combustion of sludge and other solid fuels by thermogravimetric analysis (TG) [9–13]. Zhao et al. [9] investigated the co-combustion characteristics of low-rank coal semicoke and oil sludge by the TG-FTIR method. They found that the blending of oil sludge on low-rank coal semicoke could effectively improve the ignition, burnout, and comprehensive combustion performance of blends.

Wang et al. [10] studied the co-combustion characteristics and kinetics of sewage sludge and wheat straw by thermogravimetric analysis. The results showed that blending wheat straw in sewage sludge improved the combustion performance due to the strong synergetic interaction. Chai et al. [11] found that adding waste tea into textile dyeing sludge led to higher reactivity, and the average apparent activation energy reached its minimum with 40% waste tea. The co-combustion of sludge and other solid fuels in a suitable burner to produce energy is a widely used disposal method.

Coal gasification is one of the core technologies for the clean and efficient utilization of coal, as well as the synthesis of coal-based chemicals and liquid fuels [14,15]. Gasification fine slag is the industrial solid waste from the gasification process [16]. With the rapid development of entrained-flow gasification technology, millions of tons of gasification fine slag are produced in China each year [17,18]. Due to the incomplete gasification reaction of feed coal with oxygen and water vapor in the entrained-flow gasifier, approximately 20% of the residual carbon is retained in gasification fine slag [19].

The residue carbon in the gasification fine slag can be enriched by physical methods and reused as carbon-based fuel. In recent work, Guo et al. [17] enriched the residue carbon in the coal gasification fine slag through the froth flotation method. The fixed carbon content at the dry basis of the obtained residue carbon reached 44.42%, and the higher heating value was 17.70 MJ/kg. Similarly, Guo et al. [20] also recycled residual carbon from gasification fine slag, and then it was added into bio-oil to prepare the residual carbon bio-oil slurry fuel.

It has been proven that the enriched residual carbon with low volatile content and high fixed carbon content has combustion properties comparable to low-quality coal, which is opposite to the fuel characteristics of sewage sludge [21]. Thus, the co-combustion of sewage sludge and gasification fine slag residual carbon may be a complementary and effective way to counteract the negative characteristic of individual fuel [11]. Many studies have illustrated that this promotion effect during the co-combustion process is due to the synergistic catalysis between the two fuels [10,17,22].

The alkali metal compounds in the fuel are regarded as combustion catalysts [11]. The research results of Wang et al. [22] showed that the alkali substances in biomass ash can promote the combustion of solid carbon in coal. In addition, Huang et al. [23] found that the addition of Na_2CO_3 had a significant catalytic effect on the co-combustion of sewage sludge and water hyacinth. It is important to understand the promoting effect of synergistic catalysis on the co-combustion process of fuels.

The co-combustion process may produce a variety of gaseous pollutants due to the high volatile content of the sludge [2]. Lin et al. [24] found that blending paper sludge with oil-palm solid wastes can reduce pollutant gas emissions (SO_2 , NO , and CO_2) during the co-combustion process. Cai et al. [11] also demonstrated that the co-combustions of textile dyeing sludge and waste tea reduced SO_2 emission through thermogravimetric coupled with mass spectrometry (TG-MS) analysis. It is essential to quantify the release of gaseous pollutants in the co-combustion process of sewage sludge and gasification fine slag residual carbon, which can provide important inspiration for the control of pollutants in industrial burner in the future [25–27].

The co-combustion of sewage sludge and residual carbon has great potential in the aspects of resource utilization of solid waste and application as a supplementary fuel for power generation. Unfortunately, there is no literature on the co-combustion performance of sewage sludge and gasification fine slag residual carbon until now. Therefore, it is necessary to evaluate the combustion behavior and gaseous pollutant emissions during

the co-combustion of sewage sludge and gasification fine slag residual carbon to provide a theoretical basis and useful guidance for industrial-scale application of these two solid-waste resources.

In this work, the co-combustion characteristic, synergistic catalysis, and gaseous pollutant emission patterns between sewage sludge (SS) and gasification fine slag residual carbon (RC) and their blends were comprehensively assessed using the TG-MS technique. The results could provide a vital reference for the synergetic utilization of SS and RC.

2. Results and Discussion

2.1. Combustion Behavior of SS, RC, and Their Blends

It can be seen from Figure 1a that SS, RC, and their blends display quite different weight loss curves. The weight loss curves of the blends are sandwiched between those of SS and RC, which is consistent with the results of other researchers [28,29]. In addition, the DTG curves suggest that there is only one distinct peak of reaction rate observed during the combustion of individual SS and RC and the dominating combustion stages of SS and RC are in the ranges of 200–610 °C and 500–600 °C, respectively. However, two primary stages were observed in the combustion of the SS/RC blends. The first stage is attributed to the combustion of the volatile matters and char from SS with a typical peak range of 200–500 °C. The combustion of RC and the remaining SS char mainly occurs in the second stage (500–610 °C).

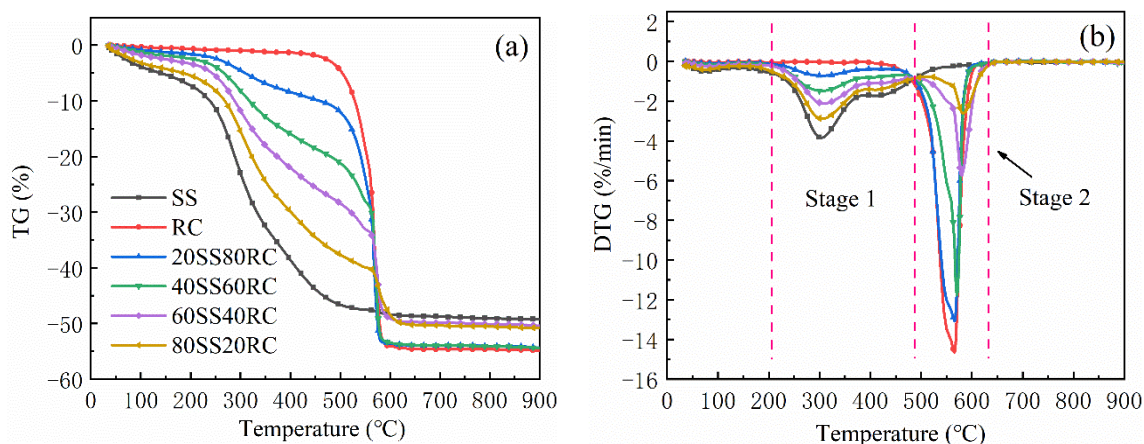


Figure 1. TG (a) and DTG (b) curves of the combustion of SS, RC, and their blends.

The parameters in Table 1 can be used to evaluate the combustion performance. The T_i of SS (221.47 °C) is much lower than that of RC (538.36 °C), which is due to the high volatile content of SS. A large number of volatile components in SS are released and burned at relatively low temperatures (Stage 1). The reason for the low volatile content of RC is that it has undergone a high-temperature gasification process exceeding 1200 °C, which results in the worse ignition property of RC. However, the I_s and I_c of RC were observed to be higher than that of SS, indicating a higher combustion stability and comprehensive combustion performance of RC. It can be concluded that the co-combustion of SS and RC may have complementary advantages to counteract the negative characteristics of individual fuel.

With the increase of SS proportion in blends, the T_i decreases from 228.32 to 223.01 °C, and the T_{m1} decreases from 311.71 to 304.49 °C, which means that the ignition property is improved and combustion is advanced. The combustion of volatile components in SS during Stage 1 can provide heat for the combustion of RC in Stage 2 and contributes to the ignition of RC [22]. Thus, the addition of SS could weaken the adverse effects of low volatile matter in RC on combustion. The T_b of blends is also decreased with the increase of SS proportion in blends, which is mainly due to the catalysis of alkali and alkaline metals in the SS ash [10].

Table 1. Combustion performances of SS, RC, and their blends.

	Samples	SS	RC	20SS80RC	40SS60RC	60SS40RC	80SS20RC
Stage 1	T_i (°C)	221.47	538.36	228.32	226.18	224.59	223.01
	T_{m1} (°C)	302.08	\	311.71	309.31	306.89	304.49
	R_{m1} (%/min)	3.85	\	0.73	1.49	2.13	2.89
Stage 2	T_{m2} (°C)	\	566.69	565.78	570.38	574.05	582.86
	R_{m2} (%/min)	\	14.55	13.07	11.77	5.75	2.62
	T_b (°C)	584.23	621.09	628.48	623.32	618.71	613.44
	R_a (%/min)	1.71	7.78	1.96	1.93	1.76	1.70
	$I_s \times 10^4$ (%·min ⁻¹ ·°C ⁻²)	0.48	3.27	1.43	1.31	0.65	0.33
	$I_c \times 10^7$ (% ² ·min ⁻² ·°C ⁻³)	2.30	6.29	7.82	7.13	3.24	1.61

The addition of SS can improve the ignition and burnout properties of RC. It is worth noting that both I_s and I_c decrease slowly with the increase of SS proportion in blends, and then they begin to drop sharply when the proportion of SS in the blends is greater than 40%. Nonetheless, when the proportion of SS in the blends is maintained below 40%, the combustion stability is still greatly improved compared with that of individual SS. The results of Parshetti et al. [30] indicated that values of I_c ($\times 10^7$) greater than 2 can be considered as having good combustion performance.

In this work, the I_c ($\times 10^7$) is higher than 2 when the proportion of SS in the blends is lower than 60%, which means that the mixing ratio of SS and RC should be controlled to meet the above requirement. Overall, the obvious complementary advantages are observed during the co-combustion of SS and RC. The co-combustion of SS and RC can not only improve the ignition and burnout property but also maintain the combustion stability and comprehensive combustion performance at a better level.

2.2. Kinetic Analysis

According to the results in Section 2.1, the co-combustion process of SS and RC at different blending proportions is mainly divided into two stages. Therefore, in order to obtain the kinetic parameters and reaction mechanisms more accurately, the two stages were analyzed separately. The kinetic parameters and models of the samples with the highest correlation coefficient are presented in Table 2. For the individual combustion of both SS and RC, the reaction mechanism follows the first-order chemical reaction model (O1).

Table 2. Kinetic parameters of SS, RC, and their blends.

Samples	Stage 1			Stage 2		
	E_a (kJ/mol)	Model	R ²	E_a (kJ/mol)	Model	R ²
SS	19.01	First-order chemical reaction (O1)	0.9812	/	/	/
RC	/	/	/	105.68	O1	0.9789
20SS80RC	33.68	O1	0.9714	55.24	O1	0.9844
40SS60RC	30.21	O1	0.9691	51.39	O1	0.9573
60SS40RC	35.82	O1	0.9828	65.15	Three-dimensional Diffusion (D3)	0.9806
80SS20RC	39.57	O1	0.9803	70.02	Three-dimensional Diffusion (D4)	0.9660

However, the E_a of RC was much higher than that of SS, which is due to the high-temperature gasification process in the gasifier that reduces the reactivity of carbon particles in RC [17]. The O1 model was also found to be the most effective mechanism for Stage 1 of the co-combustion of SS and RC. The E_a in Stage 1 decreases first and then increases with the increase of the proportion of SS in blends, while the lowest E_a (30.21 kJ/mol) was observed when the blending ratio of SS is 40%.

Different from Stage 1, the most effective mechanisms for Stage 2 changed from O1 to three-dimensional diffusion with the increase of the SS proportion in blends, which indicates that the transfer process of the reaction gas into the fuel solid particles has a great influence on Stage 2 of co-combustion when the blending ratio of SS exceeds 40%. Moreover, the increase of the SS ratio is not always beneficial to the reduction of the activation energy of the co-combustion of SS and RC. The lowest E_a (51.39 kJ/mol) in Stage 2 is also observed when the blending ratio of SS is 40%.

2.3. Synergistic Catalytic Effect Analysis

It can be seen from Figure 2a that the experimental curves of four samples are located behind the calculated curves at first and then they are ahead of the calculated curves. The difference between the experimental and calculated curves indicates that SS and RC have interaction in the co-combustion process. Variations of the interaction between SS and RC are illustrated more clearly in Figure 2b. For all the blending ratios, the antagonism effect is predominant in Stage 1. This may be attributed to the volatile content of RC being much lower than that of SS, and correspondingly its release temperature is higher than that of SS.

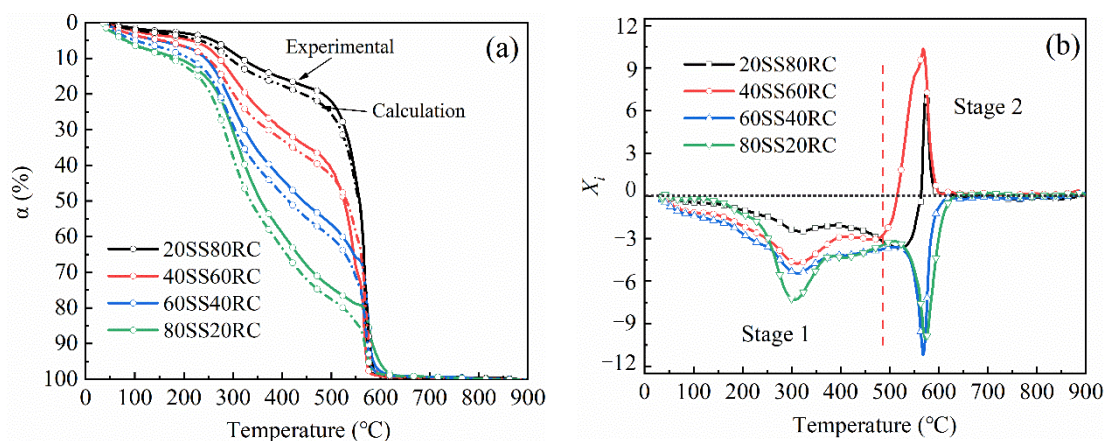


Figure 2. Comparison between the calculated and experimental conversion rate during combustion (a) and variation of the interaction index X_i at different blending ratios (b).

The heat released from the combustion of volatile components in SS was rapidly lost to RC particles, which reduces the reaction rate of SS and hinders the release of volatile components in SS [22,31]. In addition, the particle size of RC is fine, and it may cover the surface of SS particles in blends, which could also obstruct the release of volatile compounds in SS and result in a reduction of the volatile releasing rate of SS [32]. In short, the antagonism effect caused by RC is due to the heat and mass transfer limitations in Stage 1.

Moreover, the activation energies of Stage 1 (33.68–39.57 kJ/mol) in the co-combustion of SS and RC are always higher than 19.01 kJ/mol (E of the individual SS combustion), which further confirms that the antagonistic effect is dominant in the first stage. Stage 2 in co-combustion mainly includes the combustion of RC and some residual SS char. There is a significant synergistic effect when the blending ratio of SS is less than 40% in Stage 2. Such a synergistic effect could be attributed to the catalysis of alkali metals in the SS ash, which has been confirmed by many researchers [22,33–36]. In addition, the content of alkali metal in SS ash ($K_2O + Na_2O$, 12.92 wt.%) is more than twice that of RC ash (5.09 wt.%), which provides the basis for the catalytic combustion of Stage 2.

SS was demineralized to further prove the catalytic effect of alkali metals in SS during the co-combustion process. Briefly, the dried SS was mixed with the dilute hydrochloric acid solution (5 wt.%) at the solid–liquid ratio (g:mL) of 1:10 and stirred at room temperature for 2 h. Then, the demineralized SS (named DSS) was thoroughly washed with deionized water.

Finally, the SS was dried at 105 °C for 24 h in an oven. The DSS was thoroughly mixed with RC at the ratios of 40 wt.% (40DSS60RC), then the TGA experiment was carried out on 40DSS60RC according to the experimental methods described in Section 3.2. The DTG results and kinetic parameters of 40DSS60RC are provided in Figure S1 and Table S3, respectively. It can be seen from Figure S1 that the R_m of 40DSS60RC is reduced in two combustion stages compared with 40SS60RC, which suggests that the removal of alkali metals from SS leads to a decrease in the reaction rate of co-combustion. Furthermore, when the alkali metals are removed from SS, the E_a of 40DSS60RC in Stage 2 of co-combustion is significantly raised. In summary, the catalytic of alkali metals from SS can be confirmed based on the above results.

The alkali metals in the form of alkali metal salts and alkali metal oxides have an important influence on the oxygen transfer during the combustion process. The alkaline ions in the SS ash can react with the oxygen-containing alkali on the carbon surface of RC to form intricate chemical components [37]. In addition, the capacity of alkali metal salts and alkali metal oxides to absorb oxygen is relatively high [23]. The activated oxygen spills will be liberated and then react with the residual carbon in RC at a lower temperature once oxygen is absorbed by the above catalytic substances [38].

According to previous studies [2,23,37,38], the schematic diagram of the catalytic mechanism of alkali metals in the SS ash is presented in Figure 3. These catalysts accelerate the supply of oxygen to the carbon surface, and the surface of these catalysts can also provide reaction sites for the combustion of RC. This is supported by the research of Wang et al. [10]. As the proportion of SS in blends increases, Stage 1 of the co-combustion process shows obvious synergy, and the activation energy decreases, which strongly proves the catalysis of the alkali metal in the SS ash to the combustion process.

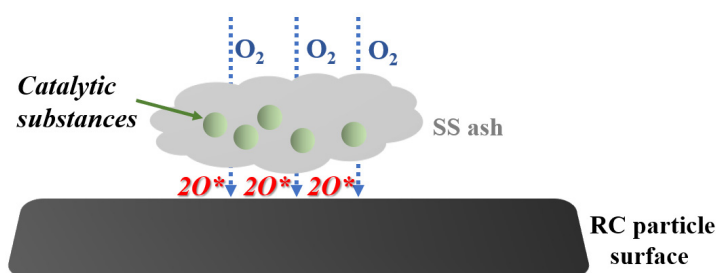


Figure 3. The suggested mechanism of the catalysis of alkali metals in the SS ash for RC combustion.

However, when the blending ratio of SS is more than 40%, the synergistic effect turns into an antagonistic effect, and the most effective mechanisms change to three-dimensional diffusion in Stage 2. This may be due to the excessive SS ash covering the RC particles, which hinders the transport of oxygen and weakens the catalytic effect of the catalytic substances in the SS ash. In summary, the blending ratio of SS is recommended to be maintained at 40% because of the lowest total activation energy ($E_a = 81.6$ kJ/mol) and the strongest synergistic catalysis ($X_i = 10.36$). The heat value of 40SS60RC is 14.865 MJ/kg (ad), which meets the requirements of heat value in waste-heat utilization [28].

2.4. Gaseous Pollutant Emissions

It is essential to clarify the release patterns of gaseous pollutants in the co-combustion process of SC and RC, which is of great significance to environmental protection and pollutant control. The emission patterns of the typical gaseous pollutants are presented in Figure 4. Normalized total gas emissions are presented in Figure 5, which were obtained from the integral areas of corresponding gas emission curves in Figure 4. Due to the low volatile content of RC, the primary occurrence mode of nitrogen is char-N. Therefore, the N-containing substances are prone to emission at relatively high temperatures.

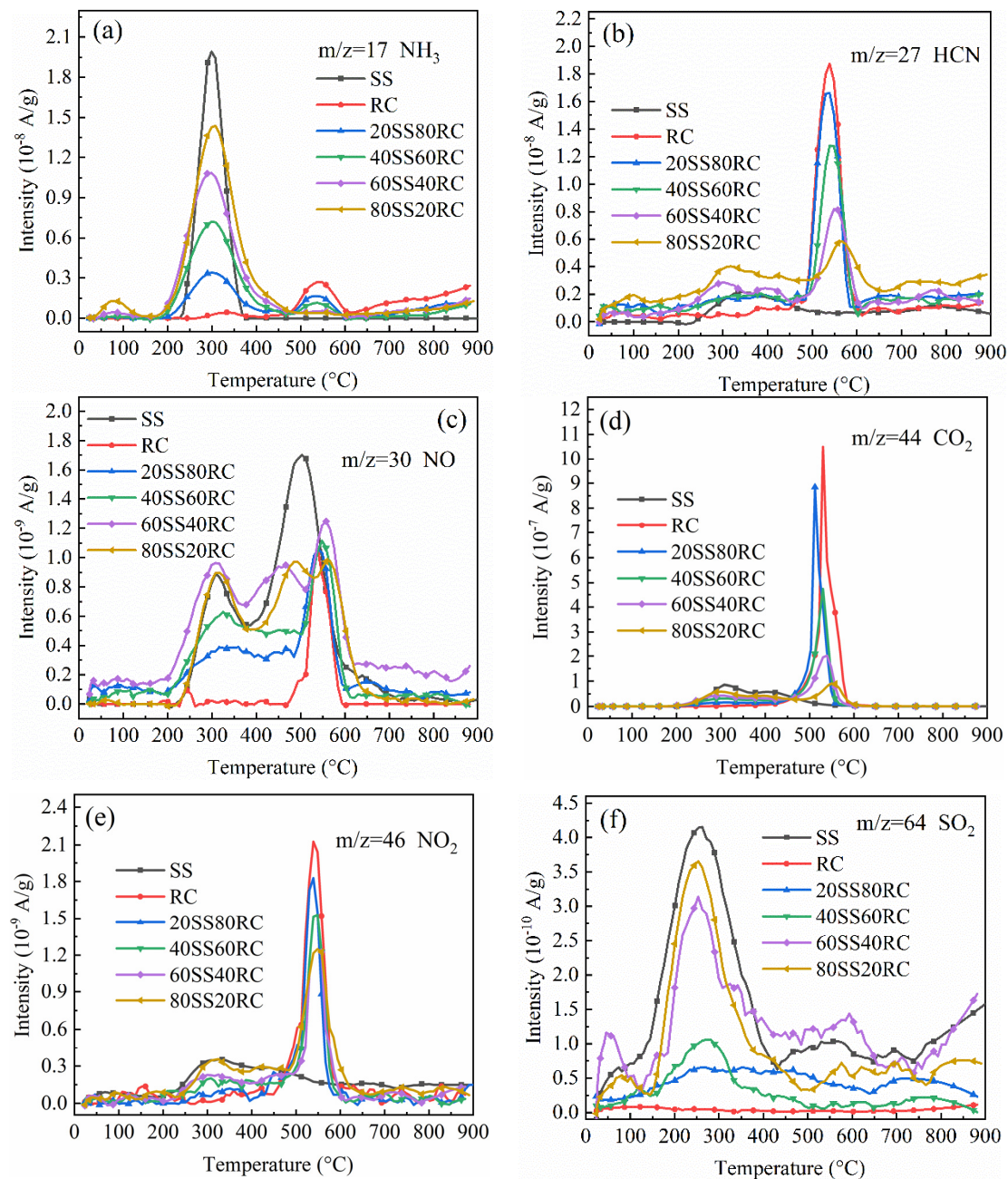


Figure 4. Gaseous pollutant emissions curves of NH_3 (a), HCN (b), NO (c), CO_2 (d), NO_2 (e), and SO_2 (f).

It can be observed from Figure 4 that the emission peaks of NH_3 , HCN , NO , and NO_2 are concentrated in the range of 500–600 °C during the combustion of individual RC, which almost coincides with the peak position of DTG curves of RC. On the contrary, there are complex N-containing substances, such as proteins, amino acids, and heterocyclic nitrogen in SS, which means that the main occurrence mode of N is volatile-N, and they tend to be released at relatively low temperatures [9]. The NO emission curve of SS displays multiple release peaks, of which the first emission peak is attributed to the decomposition of volatiles, and the second peak is due to the char combustion with N-containing substances [11].

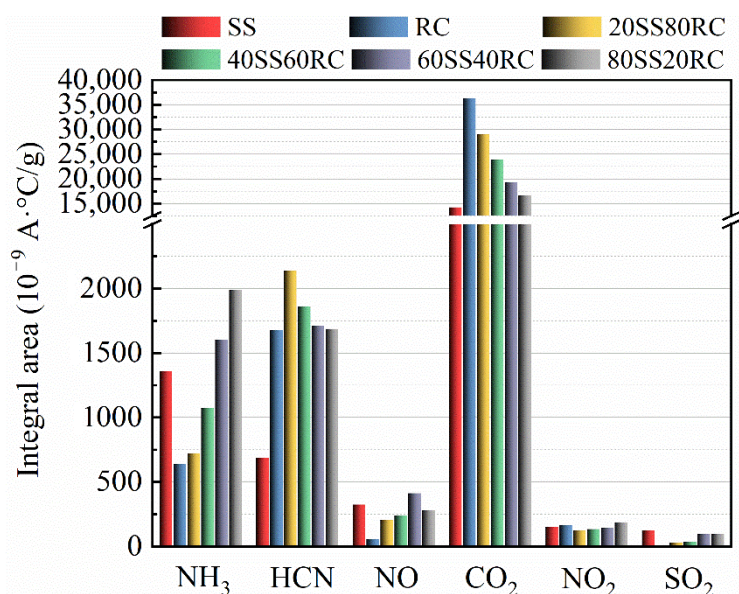


Figure 5. Integral area of gaseous pollutant emissions during the combustion process.

From Figure 5, the normalized total gas emissions of NH₃ and HCN during combustion are higher than that of both individual SS and RC at some blending ratios (e.g., 60SS40RC and 80SS20RC). This may be due to the Ca-containing substances in SS ash from Stage 1 of co-combustion catalyzing the conversion of char-N in RC to NH₃ and HCN [39]. HCN and NH₃ are considered precursors to the formation of NO_x during the combustion, and thus the normalized total gas emissions of NO_x during the combustion process increase with the increase of the SS proportion in blends [40].

Figure 4d shows the emission patterns of CO₂ during the combustion process. The emission peak of CO₂ is concentrated in the range of 500–600 °C during the combustion of individual RC, which is due to the combustion of fixed carbon in RC. Inversely, the emission peak of SS is attributed to the decomposition and combustion of the organic compounds in SS at relatively low temperatures. From Figure 5, the normalized total gas emission of CO₂ is much higher than other gas; therefore, it is the main gas product during combustion.

The difference in CO₂ emissions of SS and RC is attributed to the level of fixed carbon content, and a higher fixed carbon content suggests higher total CO₂ emission, which could well explain why the total CO₂ emission drops with the increase of the SS proportion in blends [41]. More importantly, the temperature corresponding to the two emission peaks of different blends is reduced, which suggests that the combustion is advanced and further confirms that there is a synergistic catalytic effect during the co-combustion of SS and RC. In addition, it can be observed from Figure 4f that there is almost no release of SO₂ during the entire combustion process of RC, which indicates that stable inorganic sulfur is the main occurrence mode of sulfur in RC, and this inorganic sulfur is retained in the ash after combustion [42].

The emission peak of SO₂ is around 260 °C during the combustion of individual SS, which illustrates that the sulfur in SS mainly occurs in the form of organic sulfur [11]. Thus, the pattern of sulfur emission during co-combustion of SS and RC is dominated by SS. As the mixing ratio of SS increases, the normalized total SO₂ emissions of blends rise due to the increase of sulfur content. The above results suggest that the emissions of NH₃, HCN, NO, and CO₂ are higher than SS and RC combustion alone in some mixed proportions.

Several studies also found that the addition of other fuels to sludge has a negative impact on the release of pollutant gases [11,29,43]. However, although the co-combustion of SS and RC does not appear to have any obvious advantages in the reduction of gas pollutants, the results of this study strongly confirmed the synergistic and complementary advantages of co-combustion of SS and RC. Moreover, at the recommended mixing ratio

in this work (40SS60RC), the emissions of NH_3 , NO , NO_2 , and SO_2 were all lower than those of SS and RC combustion alone. In summary, the co-combustion of SS and RC is a feasible way to convert solid waste into energy. The application of the TG-MS results to a large-scale furnace will be the focus of the following work.

3. Experimental Methods

3.1. Materials

The sewage sludge was collected from a municipal sewage treatment plant in Xuzhou City, Jiangsu Province, China. The coal gasification fine slag samples were obtained from a commercial four-nozzle entrained bed gasifier located in Ningxia Coal Industry Group Co., Ltd. of China. In this study, we attempted to enrich the residual carbon (RC) in the gasification fine slag through simple physical screening based on our previous research results [20]. The coal gasification fine slag was divided into four size fractions of 0–38 μm , 38–75 μm , 75–115 μm , and >115 μm by the wet sieving method according to Chinese standard GB/T477-2008. All the samples were dried at 105 °C for 24 h in an oven and then grounded and sieved to below 75 μm . Then, the prepared samples were sealed in a plastic bag and stored in a desiccator.

The proximate and ultimate analyses of different samples were tested according to the China National Standards GB/T 212-2008 and GB/T 476-2008. A higher heating value (HHV) was measured according to the China National Standards GB/T 213-2008. The ash chemical compositions of samples were determined according to the standard procedures of ASTM D4326-2013 and ASTM D3174-12 [44]. The proximate analyses and HHVs of the samples are presented in Table 3.

Table 3. The proximate analyses and HHV of different size fractions of CGFS.

Sample	Proximate Analysis (wt.%)				HHV (ad, MJ/kg)	Percentage of Sieved Fractions (wt.%)
	M_{ad}	A_d	V_d	FC_d *		
SS	7.93	50.85	45.74	3.41	10.79	\
CGFS	5.47	78.89	4.28	16.83	6.72	\
>115 μm	7.20	48.15	5.29	46.56	17.97	15.97
75–115 μm	0.95	88.46	2.79	8.75	4.02	9.35
38–75 μm	1.27	76.45	3.94	19.61	8.83	26.97
0–38 μm	1.38	87.11	4.68	8.21	3.84	47.89

M: moisture content; A: ash content; V: volatile content; FC: fixed carbon content; ad: air-dry basis; d: dry basis; *: by difference.

As shown in Table 3, the fraction of >115 μm had a fixed carbon content (dry basis) at 46.56%, and the HHV reached 17.97 MJ/kg, which is comparable to the fuel properties of residue carbon recovered by Guo et al. through the froth flotation method [17]. Industrial-scale classification of gasification fine slag can be used to achieve high-frequency vibrating screens and hydrocyclones in the future [45]. The RC obtained by classification was thoroughly blended with SS at the ratios of 20, 40, 60, and 80 wt.% and named 20SS80RC, 40SS60RC, 60SS40RCC, and 20RC80SS, respectively. The ultimate analyses and ash chemical compositions of SS and RC are provided in Table 4.

3.2. TG-MS Analysis

The (co-)combustion characteristics and gaseous pollutant emissions were detected by a TG-MS analyzer (Rigaku, Thermo plus EVO/Thermo Mass Photo, Tokyo, Japan). The air atmosphere of the combustion was simulated by mixing 21% O_2 with 79% He (99.99% purity gas), and the gas flow was 300 mL/min to avoid the potential interference of the air atmosphere on the detection of discharged gaseous pollutants. In each experiment, the sample (10 ± 0.5 mg) was evenly placed in a corundum crucible, and then it was heated up from room temperature to 900 °C at the heating rates of 15 °C/min with a gas flow rate of 300 mL/min.

Table 4. The ultimate analyses and ash chemical compositions of the samples.

Samples	SS	RC
Ultimate Analyses (daf, wt.%)		
C	53.39	95.01
H	7.16	2.10
O *	27.39	0.79
N	6.00	0.17
S	6.06	1.93
Ash Chemical Compositions (wt.%)		
K ₂ O	4.89	1.12
Na ₂ O	8.03	3.97
SiO ₂	16.85	39.17
Al ₂ O ₃	7.34	19.56
Fe ₂ O ₃	13.04	9.58
CaO	18.51	13.44
MgO	8.38	5.18
TiO ₂	0.56	0.92
MnO ₂	0.29	0.17

daf: dry ash-free basis; *: diff.

Before the start of each experiment, blank experiments (without samples in the corundum crucible) were conducted to obtain baselines to calibrate the errors of the instrument. The detection range of MS was a mass-to-ion ratio (m/z) of 1–150, and the scanning interval was 1 s. The main gaseous pollutants of NH₃ ($m/z = 17$), HCN ($m/z = 27$), NO ($m/z = 30$), CO₂ ($m/z = 44$), NO₂ ($m/z = 46$), and SO₂ ($m/z = 64$) were quantitatively analyzed [11,43]. All the experiments were carried out three times to ensure consistency and repeatability. The experimental error was kept within $\pm 2\%$, and the ultimate results were ascertained as the average of the three parallel results.

3.3. Combustion Performance Parameters

In order to further understand the combustion performance of samples, the TG-DTG method was employed to determine the ignition temperature (T_i) and burnout temperature (T_b) [31,46]. The maximum reaction rate (R_m) and its corresponding temperature (T_m), as well as the average reaction rate (R_a), were determined from the thermogravimetry (TG) and derivative thermogravimetry (DTG) curves.

In addition, the combustion stability index (I_s) is a measure of the stability of the combustion pathways, which can be used to obtain the degree of combustion stability of fuel based on non-isothermal TGA data [28]. The comprehensive combustion characteristic index (I_c) included the ease of ignition, the reaction rate, and the burnout temperature and is considered as a comprehensive combustion parameter to evaluate the combustibility of fuels [47]. A larger value of I_s and I_c indicates better combustibility and combustion stability of the samples. The relevant equations are as follows [28,48]:

$$I_s = \frac{R_m}{T_i \times (T_b - T_i)} \quad (1)$$

$$I_c = \frac{R_m \times R_a}{T_i^2 \times T_b} \quad (2)$$

3.4. Kinetics Model

Kinetics analysis has important guiding significance for industrial-scale production as it is the basis for scale-up and reactor design. The kinetic parameters were determined based on the non-isothermal TGA data in this study. The activation energy (E_a), reaction

mechanisms of *SS*, *RC*, and their blends during combustion were calculated using the Coats-Redfern method [17,43], which is expressed as:

$$\ln[g(\alpha)/T^2] = \ln[AR(1 - 2RT/E_a)/\delta E_a] - E_a/RT \quad (3)$$

$$\alpha = \frac{m_i - m_t}{m_i - m_f} \quad (4)$$

where α is the thermal conversion rate (%); and m_i , m_t , and m_f are the initial mass (mg), instantaneous mass at time t , and final mass after the reaction of samples, respectively. $g(\alpha)$ is the integral form of the mechanism functions (as shown in Table S1) [17,46]. T , A , R , E_a , and δ refer to the absolute temperature (K), pre-exponential factor (min^{-1}), universal gas constant (8.314 J/(K·mol)), activation energy (kJ/mol), and heating rate (K/min), respectively. In addition, $\ln[AR(1 - 2RT/E_a)/\delta E_a]$ can be considered as constant for most levels of E_a and T . Therefore, by substituting different $g(\alpha)$ into the above formula, and then plotting $\ln[g(\alpha)/T^2]$ vs. $1/T$, a fitting line with the highest correlation coefficient was acquired. Ultimately, E_a can be obtained from the slope ($-E_a/R$) of the fitting line.

3.5. Synergistic Catalytic Effect

The synergy between *SS* and *RC* has an important influence on the co-combustion reaction. In order to verify the synergy between *SS* and *RC* in the co-combustion process, the theoretical combustion conversion curves of the *SS/RC* blends and the interaction index X_i were calculated by the following formulas [17,31]:

$$\alpha_t = \beta \times \alpha_{SS} + (1 - \beta) \times \alpha_{RC} \quad (5)$$

where, α_t is the theoretical thermal conversion rate of blends with different proportions; α_{SS} and α_{RC} are the individual thermal conversion rate of *SS* and *RC*; β is the proportion of *SS* in the blends;

$$X_i = \alpha_e - \alpha_t \quad (6)$$

where α_e is the experimental thermal conversion rate of blends with different proportions. The interaction index $X_i > 0$ indicates synergy, $X_i < 0$ indicates antagonism, and $X_i = 0$ indicates no interaction.

4. Conclusions

1. Blending *SS* with *RC* effectively avoids the negative characteristics of the individual fuels. The co-combustion of *SS* and *RC* can not only improve the ignition and burnout property but also maintain the combustion stability and comprehensive combustion performance at a better level.
2. The first-order chemical reaction is the reaction mechanism for Stage 1 of the co-combustion of *SS* and *RC*, while the most effective mechanisms for Stage 2 are changed from first-order chemical reactions to three-dimensional diffusion with the increase of the *SS* proportion in blends.
3. The synergistic catalysis effect was confirmed when the blending ratio of *SS* was less than 40%, and the blending ratio of *SS* is recommended to be maintained at 40% due to the lowest activation energy and the strongest synergistic effect.
4. The emissions of gaseous pollutants corresponded to the primary combustion stages of *SS*, *RC*, and their blends. In co-combustion, the NH_3 , HCN , NO_x , and SO_2 emissions gradually rose with the increase of *SS* proportion in blends due to the high content of organic compounds in *SS*.

Supplementary Materials: The following are available online at <https://www.mdpi.com/article/10.3390/catal11101142/s1>, Table S1: Kinetic mechanism functions, Table S2: Kinetic parameters of various samples at different combustion stage, Table S3: The kinetic parameters of 40SS60RC and 40DSS60RC, Figure S1: Comparison of the DTG results of 40SS60RC and 40DSS60RC.

Author Contributions: Data curation, Y.G., J.W. and B.D.; Formal analysis, Y.G.; Funding acquisition, J.W. and Y.Z.; Investigation, W.J. and R.W.; Methodology, Y.G., F.G., G.Q. and B.D.; Project administration, J.W. and Y.Z.; Resources, W.J., G.Q. and R.W.; Software, F.G. and B.D.; Supervision, J.W.; Writing—original draft, Y.G.; Writing—review & editing, J.W., F.G., Y.Z. and B.D. All authors have read and agreed to the published version of the manuscript.

Funding: This work was funded by the Natural Science Foundation of Shandong Province (No. ZR2020KE044), the National Natural Science Foundation of China (No. 51974311), the National Key Research and Development Program of China (No. 2019YFC1904302), and the Open Sharing Fund for the Large-scale Instruments and Equipment of China University of Mining and Technology (CUMT) (No. DYGX-2021-075).

Data Availability Statement: Data is contained within the article or Supplementary Material.

Conflicts of Interest: The authors declare no conflict of interest.

References

1. Xiong, Q.; Wu, X.; Lv, H.; Liu, S.; Hou, H.; Wu, X. Influence of rice husk addition on phosphorus fractions and heavy metals risk of biochar derived from sewage sludge. *Chemosphere* **2021**, *280*, 130566. [[CrossRef](#)]
2. Liu, J.; Huang, L.; Sun, G.; Chen, J.; Zhuang, S.; Chang, K.; Xie, W.; Kuo, J.; He, Y.; Sun, S. (Co-) combustion of additives, water hyacinth and sewage sludge: Thermogravimetric, kinetic, gas and thermodynamic modeling analyses. *Waste Manag.* **2018**, *81*, 211–219. [[CrossRef](#)] [[PubMed](#)]
3. Naqvi, S.R.; Tariq, R.; Shahbaz, M.; Naqvi, M.; Amin, A.; Khan, Z.; Mackey, H.; McKay, G.; Al-Ansari, T. Recent Developments on Sewage Sludge Pyrolysis and its Kinetics: Resources Recovery, Thermogravimetric Platforms, and Innovative Prospects. *Comput. Chem. Eng.* **2021**, *150*, 107325. [[CrossRef](#)]
4. Bulavchenko, O.A.; Saraev, A.A.; Kremneva, A.M.; Shashkov, M.V.; Zaikina, O.O.; Gulyaeva, Y.K.; Grachev, A.N.; Kikhtyanin, O.; Kubička, D.; Yakovlev, V.A. Effect of Temperature on the Hydrotreatment of Sewage Sludge-Derived Pyrolysis Oil and Behavior of Ni-Based Catalyst. *Catalysts* **2020**, *10*, 1273. [[CrossRef](#)]
5. Celary, P.; Sobik-Szołtysek, J. Vitrification as an alternative to landfilling of tannery sewage sludge. *Waste Manag.* **2014**, *34*, 2520–2527. [[CrossRef](#)]
6. Wei, L.; Zhu, F.; Li, Q.; Xue, C.; Xia, X.; Yu, H.; Zhao, Q.; Jiang, J.; Bai, S. Development, current state and future trends of sludge management in China: Based on exploratory data and CO₂-equivalent emissions analysis. *Environ. Int.* **2020**, *144*, 106093. [[CrossRef](#)]
7. Kosowska-Golachowska, M.; Luckos, A.; Kijo-Kleczkowska, A.; Musiał, T.; Wolski, K.; Środa, K. Gaseous emissions during oxy-fuel combustion of sewage sludge in a circulating fluidized bed. *Powder Technol.* **2020**, *371*, 209–216. [[CrossRef](#)]
8. Modaresi, Z.K.; Karimi, G.; Mowla, D. Study of co-combustion of dried sewage sludge with coke: Thermogravimetric assessment and gaseous emissions. *J. Environ. Chem. Eng.* **2019**, *7*, 102871. [[CrossRef](#)]
9. Zhao, R.; Qin, J.; Chen, T.; Wang, L.; Wu, J. Experimental study on co-combustion of low rank coal semicoke and oil sludge by TG-FTIR. *Waste Manag.* **2020**, *116*, 91–99. [[CrossRef](#)]
10. Wang, C.; Wang, X.; Jiang, X.; Li, F.; Lei, Y.; Lin, Q. The thermal behavior and kinetics of co-combustion between sewage sludge and wheat straw. *Fuel Process. Technol.* **2019**, *189*, 1–14. [[CrossRef](#)]
11. Cai, H.; Liu, J.; Kuo, J.; Buyukada, M.; Evrendilek, F. Thermal characteristics, kinetics, gas emissions and thermodynamic simulations of (co-) combustions of textile dyeing sludge and waste tea. *J. Clean. Prod.* **2019**, *239*, 118113. [[CrossRef](#)]
12. Huang, L.; Liu, J.; He, Y.; Sun, S.; Chen, J.; Sun, J.; Chang, K.; Kuo, J. Thermodynamics and kinetics parameters of co-combustion between sewage sludge and water hyacinth in CO₂/O₂ atmosphere as biomass to solid biofuel. *Bioresour. Technol.* **2016**, *218*, 631–642. [[CrossRef](#)] [[PubMed](#)]
13. Hu, S.; Ma, X.; Lin, Y.; Yu, Z.; Fang, S. Thermogravimetric analysis of the co-combustion of paper mill sludge and municipal solid waste. *Energy Convers. Manag.* **2015**, *99*, 112–118. [[CrossRef](#)]
14. Jiang, P.; Xie, C.-R.; Luo, C.-L.; Meng, W.; Yang, G.; Yu, G.-S.; Gong, Y.; Xu, M.; Wu, T. Distribution and modes of occurrence of heavy metals in opposed multi-burner coal-water-slurry gasification plants. *Fuel* **2021**, *303*, 121163. [[CrossRef](#)]
15. Dai, B.; Zhang, L.; Cui, J.-F.; Hoadley, A.; Zhang, L. Integration of pyrolysis and entrained-bed gasification for the production of chemicals from Victorian brown coal—Process simulation and exergy analysis. *Fuel Process. Technol.* **2017**, *155*, 21–31. [[CrossRef](#)]
16. Guo, F.; Liu, H.; Zhao, X.; Guo, Y.; Guo, Z.; Miao, Z.; Zhang, Y.; Li, J.; Wu, J. Insights on water temporal-spatial migration laws of coal gasification fine slag filter cake during water removal process and its enlightenment for efficient dewatering. *Fuel* **2021**, *292*, 120274. [[CrossRef](#)]
17. Guo, Y.; Guo, F.; Zhou, L.; Guo, Z.; Miao, Z.; Liu, H.; Zhang, X.; Wu, J.; Zhang, Y. Investigation on co-combustion of coal gasification fine slag residual carbon and sawdust char blends: Physicochemical properties, combustion characteristic and kinetic behavior. *Fuel* **2021**, *292*, 120387. [[CrossRef](#)]
18. Zhang, Y.; Zhou, L.; Chen, L.; Guo, Y.; Guo, F.; Wu, J.; Dai, B. Synthesis of zeolite Na-P1 from coal fly ash produced by gasification and its application as adsorbent for removal of Cr (VI) from water. *Front. Chem. Sci. Eng.* **2020**, *15*, 518–527. [[CrossRef](#)]

19. Gu, Y.-Y.; Qiao, X.-C. A carbon silica composite prepared from water slurry coal gasification slag. *Microporous Mesoporous Mater.* **2019**, *276*, 303–307. [[CrossRef](#)]
20. Guo, F.; Guo, Y.; Guo, Z.; Miao, Z.; Zhao, X.; Zhang, Y.; Li, J.; Wu, J. Recycling Residual Carbon from Gasification Fine Slag and Its Application for Preparing Slurry Fuels. *ACS Sustain. Chem. Eng.* **2020**, *8*, 8830–8839. [[CrossRef](#)]
21. Dai, G.; Zheng, S.; Wang, X.; Bai, Y.; Dong, Y.; Du, J.; Sun, X.; Tan, H. Combustibility analysis of high-carbon fine slags from an entrained flow gasifier. *J. Environ. Manag.* **2020**, *271*, 111009. [[CrossRef](#)] [[PubMed](#)]
22. Wang, G.; Zhang, J.; Shao, J.; Liu, Z.; Zhang, G.; Xu, T.; Guo, J.; Wang, H.; Xu, R.; Lin, H. Thermal behavior and kinetic analysis of co-combustion of waste biomass/low rank coal blends. *Energy Convers. Manag.* **2016**, *124*, 414–426. [[CrossRef](#)]
23. Huang, L.; Xie, C.; Liu, J.; Zhang, X.; Chang, K.; Kuo, J.; Sun, J.; Xie, W.; Zheng, L.; Sun, S. Influence of catalysts on co-combustion of sewage sludge and water hyacinth blends as determined by TG-MS analysis. *Bioresour. Technol.* **2018**, *247*, 217–225. [[CrossRef](#)]
24. Lin, Y.; Ma, X.; Ning, X.; Yu, Z. TGA–FTIR analysis of co-combustion characteristics of paper sludge and oil-palm solid wastes. *Energy Convers. Manag.* **2015**, *89*, 727–734. [[CrossRef](#)]
25. Yu, D.; Chen, M.; Wei, Y.; Niu, S.; Xue, F. An assessment on co-combustion characteristics of Chinese lignite and eucalyptus bark with TG–MS technique. *Powder Technol.* **2016**, *294*, 463–471. [[CrossRef](#)]
26. Duan, X.; Dou, J.; Zhao, Y.; Khoshk Rish, S.; Yu, J. A Study on Mn-Fe Catalysts Supported on Coal Fly Ash for Low-Temperature Selective Catalytic Reduction of NO_x in Flue Gas. *Catalysts* **2020**, *10*, 1399. [[CrossRef](#)]
27. Gao, F.; Toops, T.J. Selective Catalytic Reduction: From Basic Science to deNO_x Applications. *Catalysts* **2021**, *11*, 250. [[CrossRef](#)]
28. Wang, T.; Hou, H.; Ye, Y.; Rong, H.; Li, J.; Xue, Y. Combustion behavior of refuse-derived fuel produced from sewage sludge and rice husk/wood sawdust using thermogravimetric and mass spectrometric analyses. *J. Clean. Prod.* **2019**, *222*, 1–11. [[CrossRef](#)]
29. Xie, W.; Huang, J.; Liu, J.; Zhao, Y.; Chang, K.; Kuo, J.; He, Y.; Sun, J.; Zheng, L.; Xie, W. Assessing thermal behaviors and kinetics of (co-) combustion of textile dyeing sludge and sugarcane bagasse. *Appl. Therm. Eng.* **2018**, *131*, 874–883. [[CrossRef](#)]
30. Parshetti, G.K.; Quek, A.; Betha, R.; Balasubramanian, R. TGA–FTIR investigation of co-combustion characteristics of blends of hydrothermally carbonized oil palm biomass (EFB) and coal. *Fuel Process. Technol.* **2014**, *118*, 228–234. [[CrossRef](#)]
31. Tong, W.; Liu, Q.; Ran, G.; Liu, L.; Ren, S.; Chen, L.; Jiang, L. Experiment and expectation: Co-combustion behavior of anthracite and biomass char. *Bioresour. Technol.* **2019**, *280*, 412–420. [[CrossRef](#)]
32. Xinjie, L.; Shihong, Z.; Xincheng, W.; Jinai, S.; Xiong, Z.; Xianhua, W.; Haiping, Y.; Hanping, C. Co-combustion of wheat straw and camphor wood with coal slime: Thermal behaviour, kinetics, and gaseous pollutant emission characteristics. *Energy* **2021**, 121292. [[CrossRef](#)]
33. Le Manquais, K.; Snape, C.; Barker, J.; McRobbie, I. TGA and drop tube furnace investigation of alkali and alkaline earth metal compounds as coal combustion additives. *Energy Fuels* **2012**, *26*, 1531–1539. [[CrossRef](#)]
34. Li, X.; Ma, B.; Xu, L.; Luo, Z.; Wang, K. Catalytic effect of metallic oxides on combustion behavior of high ash coal. *Energy Fuels* **2007**, *21*, 2669–2672. [[CrossRef](#)]
35. Farrow, T.S.; Sun, C.; Snape, C.E. Impact of biomass char on coal char burn-out under air and oxy-fuel conditions. *Fuel* **2013**, *114*, 128–134. [[CrossRef](#)]
36. Qi, X.; Song, G.; Song, W.; Yang, S.; Lu, Q. Combustion performance and slagging characteristics during co-combustion of Zhundong coal and sludge. *J. Energy Inst.* **2018**, *91*, 397–410. [[CrossRef](#)]
37. Zhaosheng, Y.; Xiaoqian, M.; Ao, L. Thermogravimetric analysis of rice and wheat straw catalytic combustion in air-and oxygen-enriched atmospheres. *Energy Convers. Manag.* **2009**, *50*, 561–566. [[CrossRef](#)]
38. Shen, B. Study on MSW catalytic combustion by TGA. *Energy Convers. Manag.* **2006**, *47*, 1429–1437. [[CrossRef](#)]
39. Tsubouchi, N.; Ohtsuka, Y. Nitrogen chemistry in coal pyrolysis: Catalytic roles of metal cations in secondary reactions of volatile nitrogen and char nitrogen. *Fuel Process. Technol.* **2008**, *89*, 379–390. [[CrossRef](#)]
40. Wang, T.; Fu, T.; Chen, K.; Cheng, R.; Chen, S.; Liu, J.; Mei, M.; Li, J.; Xue, Y. Co-combustion behavior of dyeing sludge and rice husk by using TG-MS: Thermal conversion, gas evolution, and kinetic analyses. *Bioresour. Technol.* **2020**, *311*, 123527. [[CrossRef](#)]
41. Hu, J.; Song, Y.; Liu, J.; Evrendilek, F.; Buyukada, M.; Yan, Y.; Li, L. Combustions of torrefaction-pretreated bamboo forest residues: Physicochemical properties, evolved gases, and kinetic mechanisms. *Bioresour. Technol.* **2020**, *304*, 122960. [[CrossRef](#)] [[PubMed](#)]
42. Ren, X.; Sun, R.; Meng, X.; Vorobiev, N.; Schiemann, M.; Levendis, Y.A. Carbon, sulfur and nitrogen oxide emissions from combustion of pulverized raw and torrefied biomass. *Fuel* **2017**, *188*, 310–323. [[CrossRef](#)]
43. Huang, J.; Liu, J.; Kuo, J.; Xie, W.; Zhang, X.; Chang, K.; Buyukada, M.; Evrendilek, F. Kinetics, thermodynamics, gas evolution and empirical optimization of (co-) combustion performances of spent mushroom substrate and textile dyeing sludge. *Bioresour. Technol.* **2019**, *280*, 313–324. [[CrossRef](#)] [[PubMed](#)]
44. Dai, B.; Wu, X.; Zhang, J.; Ninomiya, Y.; Yu, D.; Zhang, L. Characteristics of iron and sulphur in high-ash lignite (Pakistani lignite) and their influence on long-term T23 tube corrosion under super-critical coal-fired boiler conditions. *Fuel* **2020**, *264*, 116855. [[CrossRef](#)]
45. Li, F.; Liu, P.; Yang, X.; Zhang, Y.; Li, X.; Jiang, L.; Wang, H.; Fu, W. Purification of granular sediments from wastewater using a novel hydrocyclone. *Powder Technol.* **2021**, *393*, 751–763. [[CrossRef](#)]
46. Guo, F.; He, Y.; Hassanpour, A.; Gardy, J.; Zhong, Z. Thermogravimetric analysis on the co-combustion of biomass pellets with lignite and bituminous coal. *Energy* **2020**, *197*, 117147. [[CrossRef](#)]

-
47. Guo, F.; Zhong, Z. Optimization of the co-combustion of coal and composite biomass pellets. *J. Clean. Prod.* **2018**, *185*, 399–407. [[CrossRef](#)]
 48. Liu, H.; Liu, J.; Huang, H.; Evrendilek, F.; He, Y.; Buyukada, M. Combustion parameters, evolved gases, reaction mechanisms, and ash mineral behaviors of durian shells: A comprehensive characterization and joint-optimization. *Bioresour. Technol.* **2020**, *314*, 123689. [[CrossRef](#)]